Supporting Information

Self-Standing Covalent Organic Framework Membranes for H_2/CO_2 Separation

Baoju Li, Zitao Wang, Zhuangzhuang Gao, Jinquan Suo, Ming Xue, Yushan Yan, Valentin Valtchev, Shilun Qiu, and Qianrong Fang**

General Considerations

Commercially available reagents and solvents were purchased in high purity and used without purification. A Bruker AV-400 NMR spectrometer was applied to record the liquid ^{1}H NMR spectra. The PXRD data were collected on a PANalytical B.V. Empyrean powder diffractometer using a Cu Kα source (λ = 1.5418 Å) over the range of 2θ = 2.0−40.0° with a step size of 0.02° and 2s per step. The FTIR spectra (KBr) were obtained using a SHIMADZU IRAffinity-1 Fourier transform infrared spectrophotometer. The TGA analyses were carried out under nitrogen flow on a SHIMADZU DTG-60 thermal analyzer at a heating rate of 5 ºC min^{-1} from 30 to 700 °C. The N_2 adsorption-desorption isotherm was measured in a Quantachrome Autosorb-IQ analyzer with ultra-high-purity N_2 (99.999% purity). To estimate the surface area, the Brunauer-Emmett-Teller (BET) method was applied, while nonlocal density functional theory (NL-DFT) using QSDFT model was adopted to determine the pore size distributions. The SEM images were collected on JEOL JSM6700 scanning electron microscope.

Experimental Procedures

Synthesis of tetra(4-aminophenyl)methane (TAPM)[1]

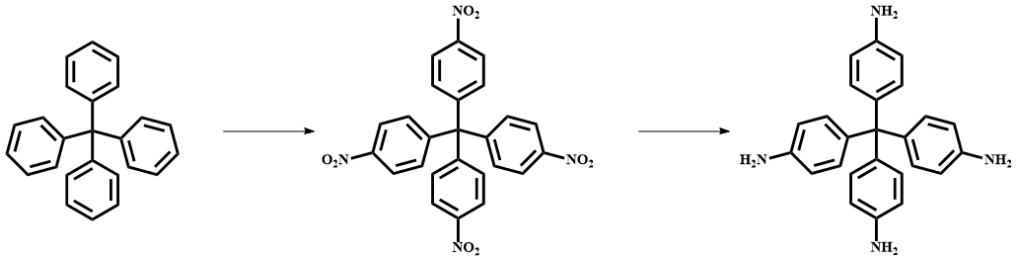

Tetrakis(4-nitrophenyl)methane (TNPM). Tetraphenylmethane (11.0 mmol) was added into fuming nitric acid (20.0 mL) at -40 ℃ under vigorous stirring. Then acetic anhydride (12.5 mL) and acetic acid (12.0 mL) were slowly added and stirred for 10 h. After filtration, the precipitate was washed with H_2O and dried at 60 ℃ under vacuum for 10 h. The resultant yellow solid was used directly for the next step without further purification.

Tetrakis(4-aminophenyl)methane (TAPM). TNPM (2.0 mmol) was added to 20.0 mL of tetrahydrofuran then hydrazine monohydrate (1.5 mL) and Raney Ni (~1.0 g) were added. After heating at 60 ℃ until all hydrazine was quenched, the mixture was cooled to room temperature and then filtered. The filtrate was concentrated by rotary evaporation to remove the solvent, and TAPM was obtained as a white solid in quantitative yield. ^{1}H NMR (d6-DMSO, 400 MHz) δ 4.83 (s, 8 H), 6.33-6.42 (m, 8 H), 6.65-6.72 (m, 8 H); 13C NMR (d_6-DMSO, 100 MHz) δ 61.09, 112.55, 131.01, 135.82, 145.63.

Preparation of self-standing COF membranes

COF-300 membrane. TAPM (0.4 mmol, 152 mg) and terephthaldehyde (TPA, 0.8 mmol, 108 mg) were placed in a mortar grounded using a pestle to mix them uniformly. Afterwards, 2mmol of ammonium acetate (154 mg) was added to continue grinding evenly, and a few drops of deionized water was added during the process to form a solid-liquid blend and put it into a depth 1 mm, diameter 15 mm, round mold and pressed flat with a glass sheet. Finally, the mold was placed horizontally face up in a Teflon-lined stainless-steel autoclave, which was filled with 15 mL 1,4-dioxane and 3 mL 6 M acetic acid. Above process takes place in the glove box. The mold without direct contact with dioxane and acetic acid solution, and the reaction lasted for 72 h at 120 °C.

N-COF membrane. 1,3,5-triformylbenzene (BTCA) (0.4 mmol, 65 mg) and tris(4-aminotriphenyl)amine (TAPA, 0.4 mmol, 116 mg) were placed in a mortar grounded using a pestle to mix them uniformly. Afterwards, 2mmol of ammonium acetate (154 mg) was added to continue grinding evenly, and a few drops of deionized water was added during the process to form a solid-liquid blend and put it into a depth 1 mm, diameter 15 mm, round mold and pressed flat with a glass sheet. Finally, the mold was placed horizontally face up in a Teflon-lined stainless-steel autoclave, which was filled with 15 mL 1,4-dioxane and 3 mL 6 M acetic acid. Above process takes place in the glove box. The mold without direct contact with dioxane and acetic acid solution, and the reaction lasted for 72 h at 120 °C.

Gas-Separation Tests

Gas permeation of the resultant membrane was conducted in a Wicke−Kallenbach system. For the single gas permeation measurement, H_2, CO_2, CH_4 as the feed gas were set to 50 mL min^{-1}, Ar was used as sweep gas was set to 50 mL min^{-1} and the pressures at both sides were kept at 1 bar. For the mixed gas permeation measurement, a 1:1 mixture of gas was applied to the feed side of the membrane, and the feed flow rate was kept constant at 100 mL min^{-1} (each gas of 50 mL min^{-1}). Pressures at both sides were constant at 1 bar, and the Ar (50 mL min^{-1}) was used as sweep gas. A calibrated gas chromatography (GC-2014C, SHIMAZU) was employed as a real-time monitor, analyzing the composition of permeated gas. Membrane permeance, P_i (mol m^2 s^{-1} $Pa^{-1)}$, can be calculated by

$$P_i = \frac{N_i}{\Delta P_i \times A}$$

where N_i (mol s^{-1}) is the permeate rate of component i, ΔP_i (Pa) is the trans-membrane pressure difference of component i, and A (m^2) is the effective area of membrane. The unit GPU is used for the gas permeance, where 1GPU = 3.3928× 10^{-10} mol m^{-2} s^{-1} Pa^{-1}.

The selectivity (or separation factor) $\alpha_{i,j}$ of an equimolar binary gas mixture can be calculated by

$$\alpha_{i,j} = \frac{X_i / X_j}{Y_i / Y_j}$$

Where X and Y are the molar fractions of the corresponding component i, j in the permeate and feed side, respectively.

Supplementary Characterization and Performance Data

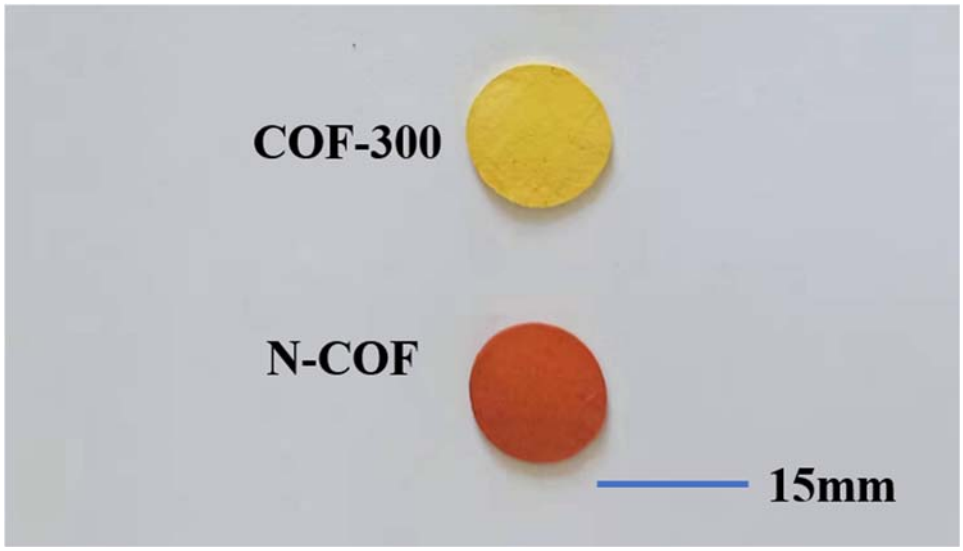

Figure S1. Optical pictures of COF-300 membrane (top) and N-COF membrane (bottom).

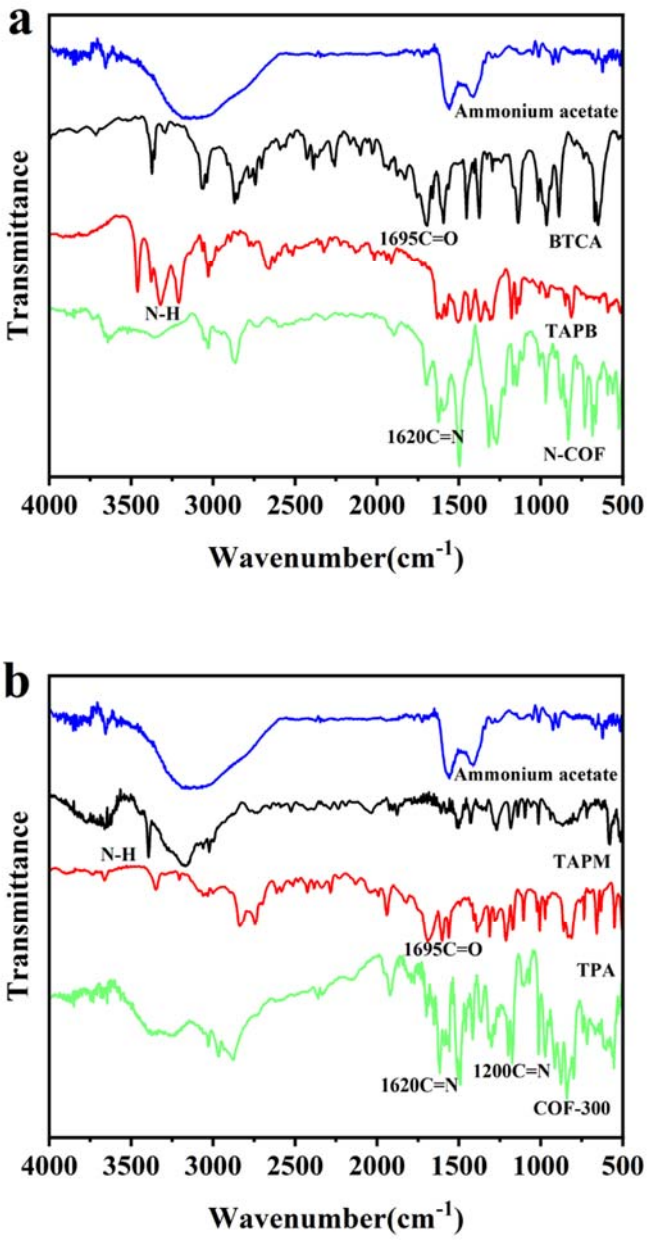

Figure S2. FTIR spectra of (a) N-COF membrane and (b) COF-300 membrane.

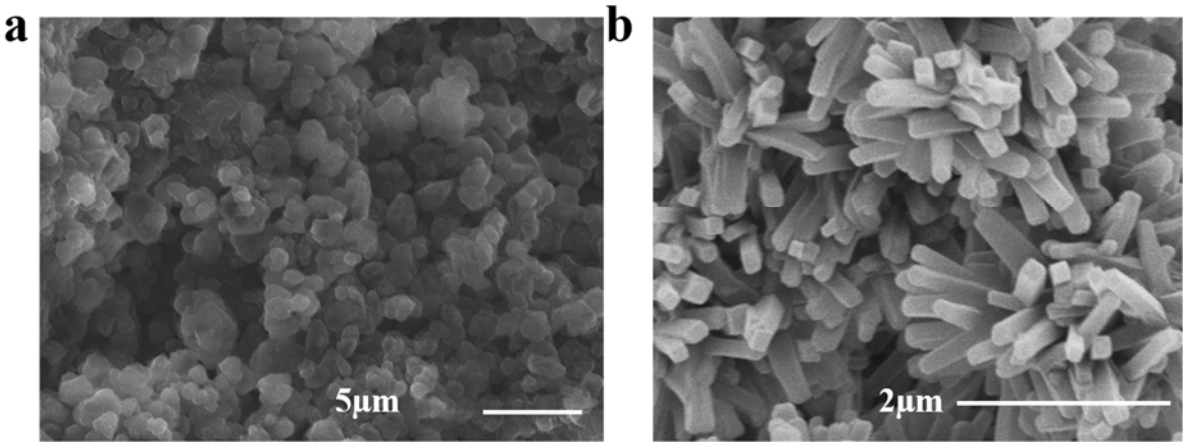

Figure S3. Zoomed view of cross-section SEM image of (a) N-COF membrane and (b) COF-300 membrane.

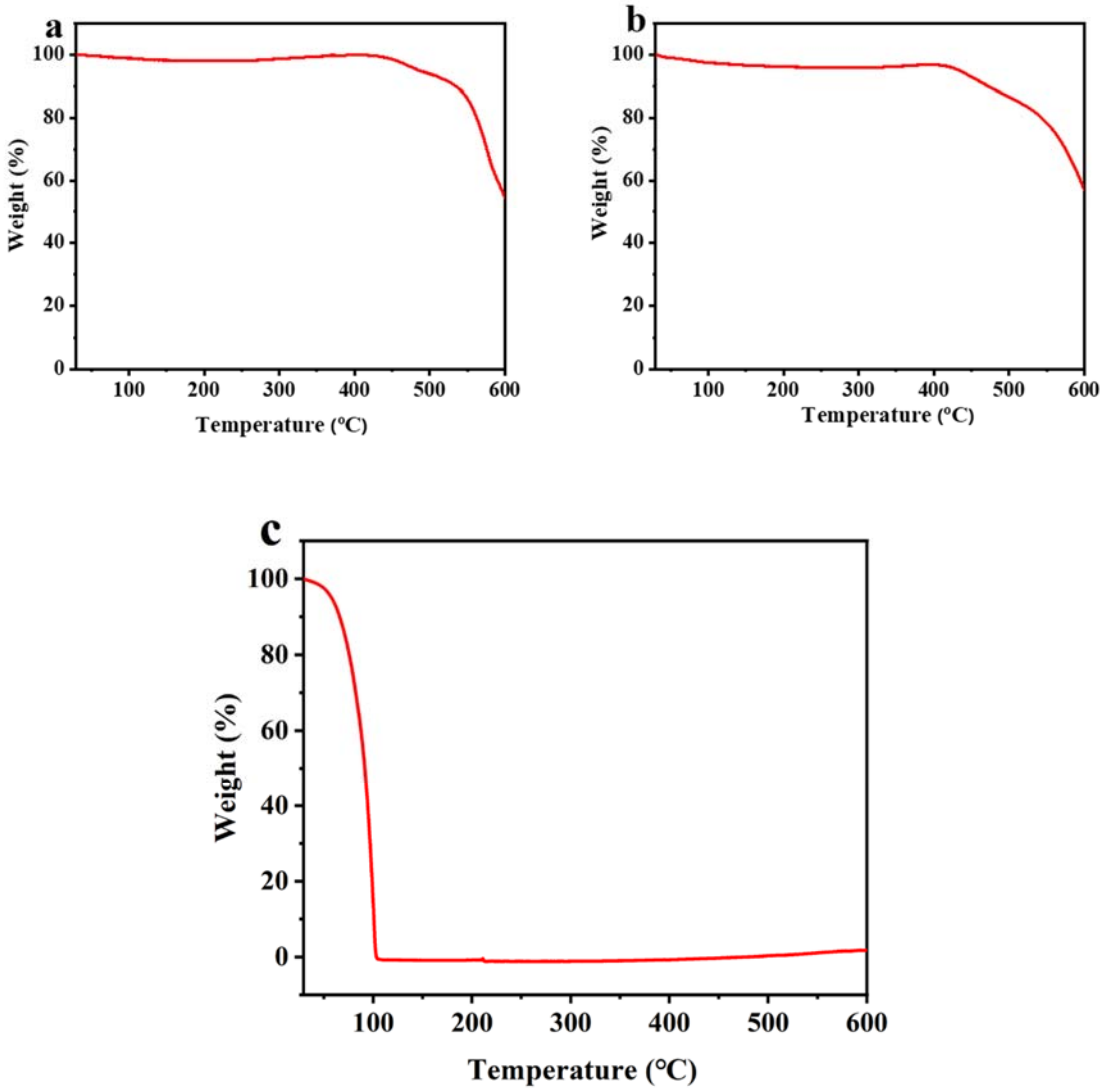

Figure S4. TGA curves of (a) N-COF membrane, (b) COF-300 membrane, and (c) ammonium acetate.

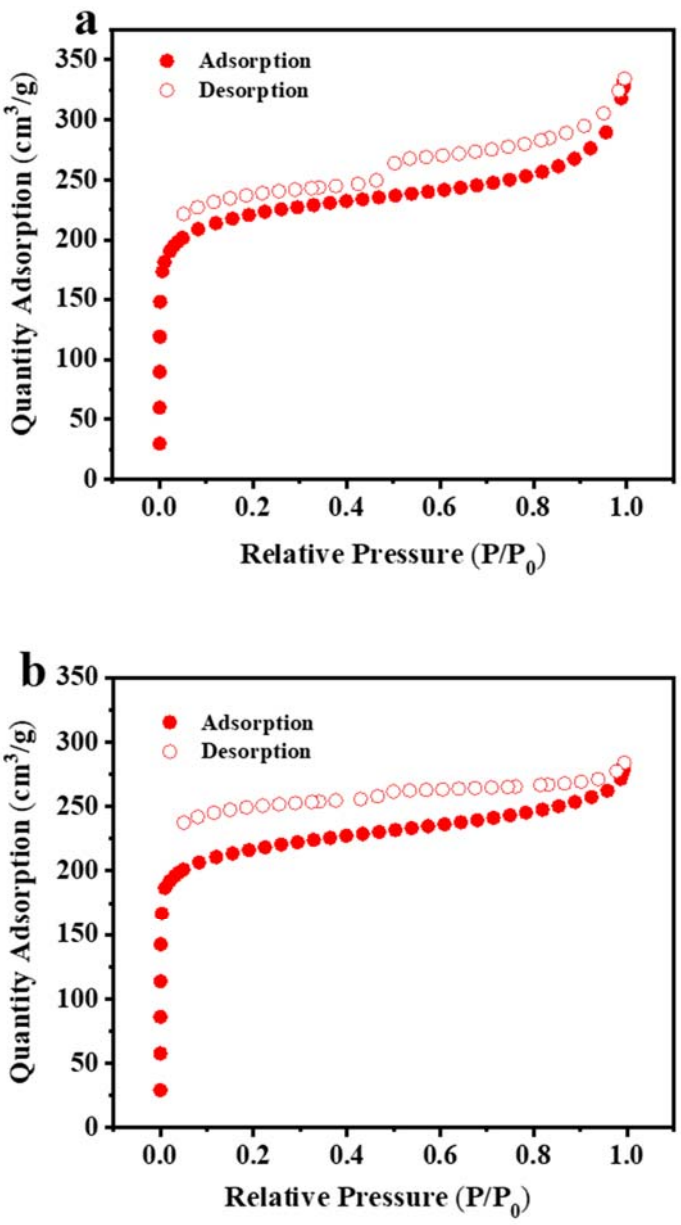

Figure S5. N_2 adsorption-desorption isotherms of (a) N-COF membrane and (b) COF-300 membrane.

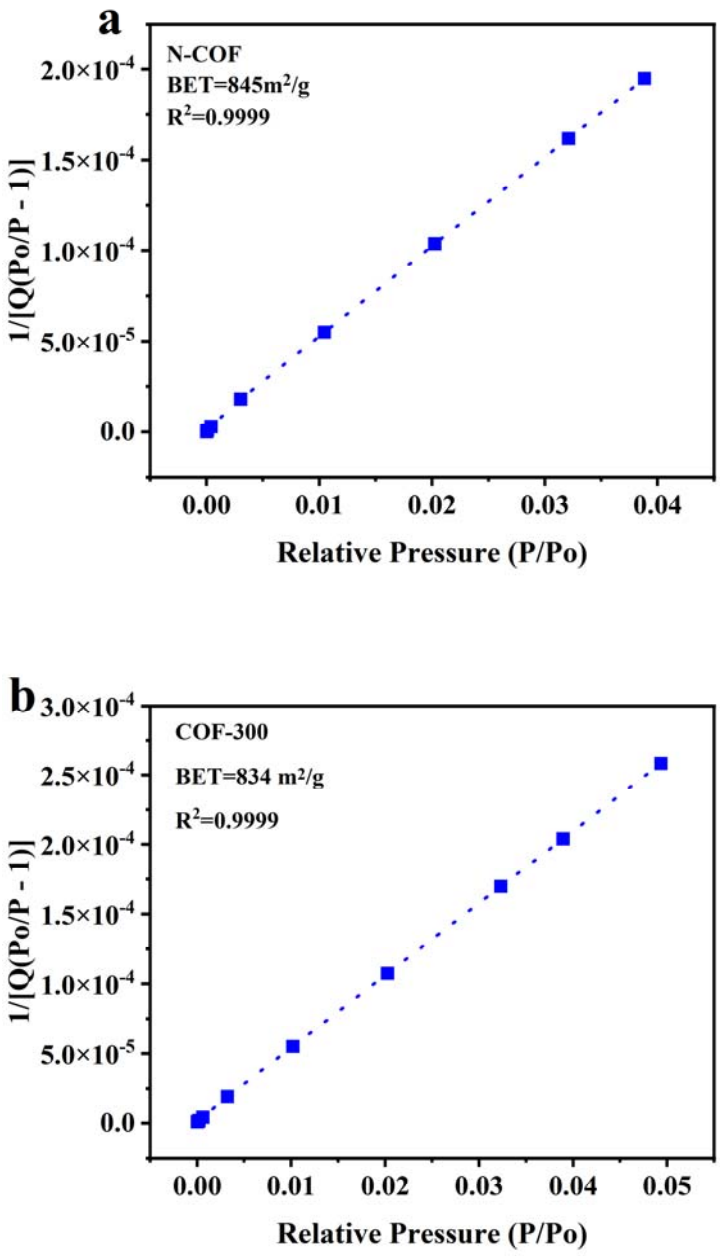

Figure S6. BET plots of (a) N-COF membrane and (b) COF-300 membrane.

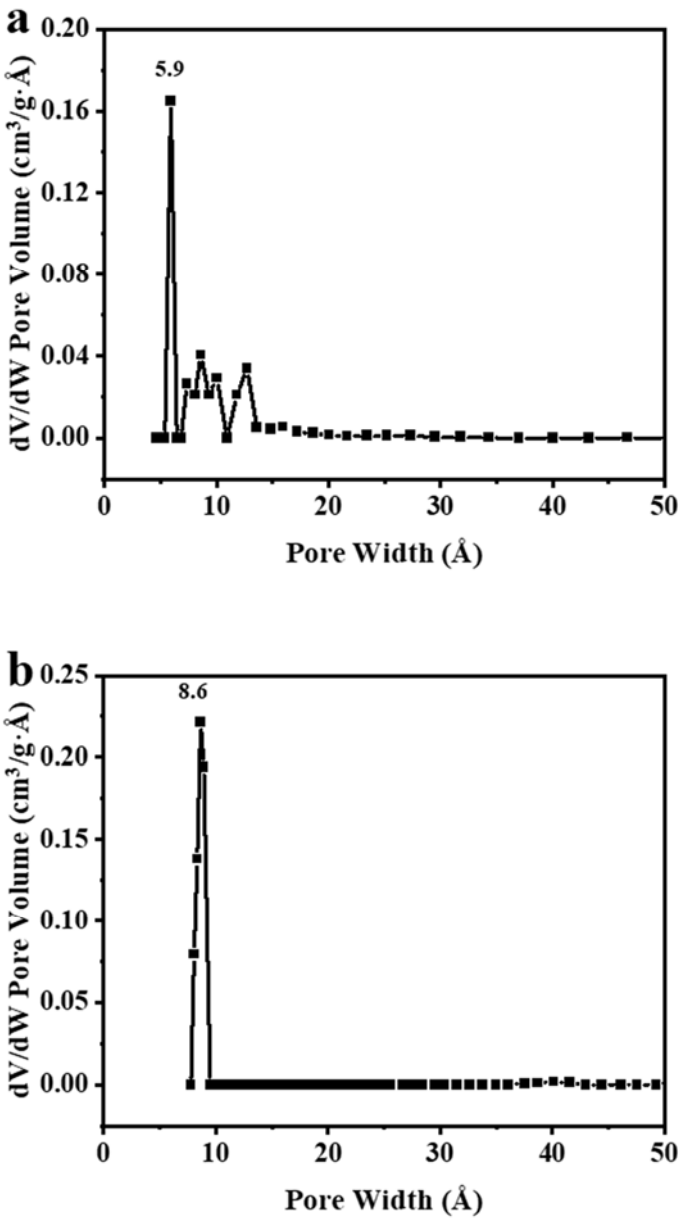

Figure S7. Pore-size distribution calculated by fitting on the NLDFT model to the adsorption data of (a) N-COF membrane and (b) COF-300 membrane.

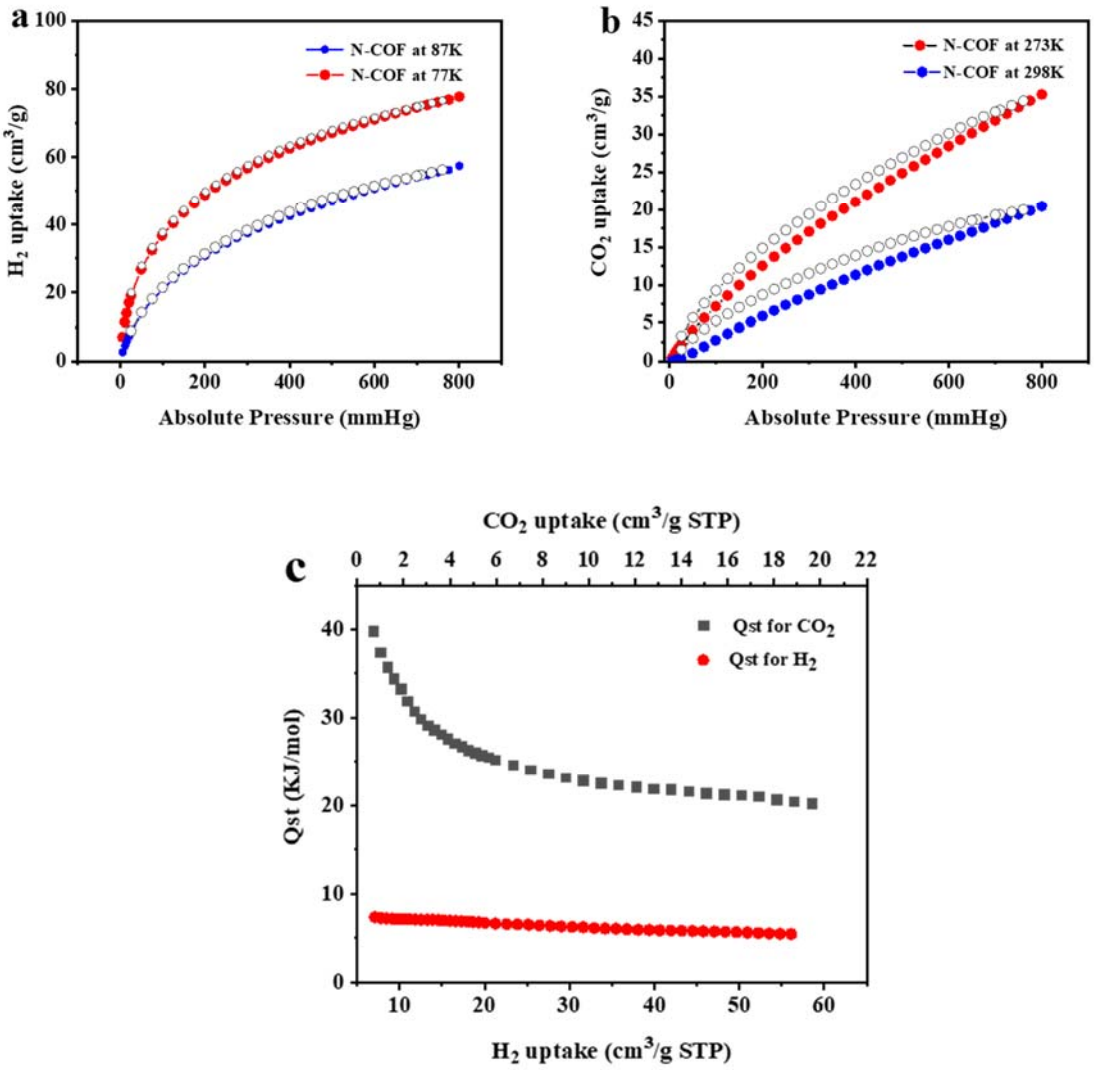

Figure S8. (a) H_2 adsorption isotherms of N-COF membrane. (b) CO_2 adsorption isotherms of N-COF membrane. (c) Isosteric heat of adsorption (Qst) of H_2 and CO_2 for N-COF membrane.

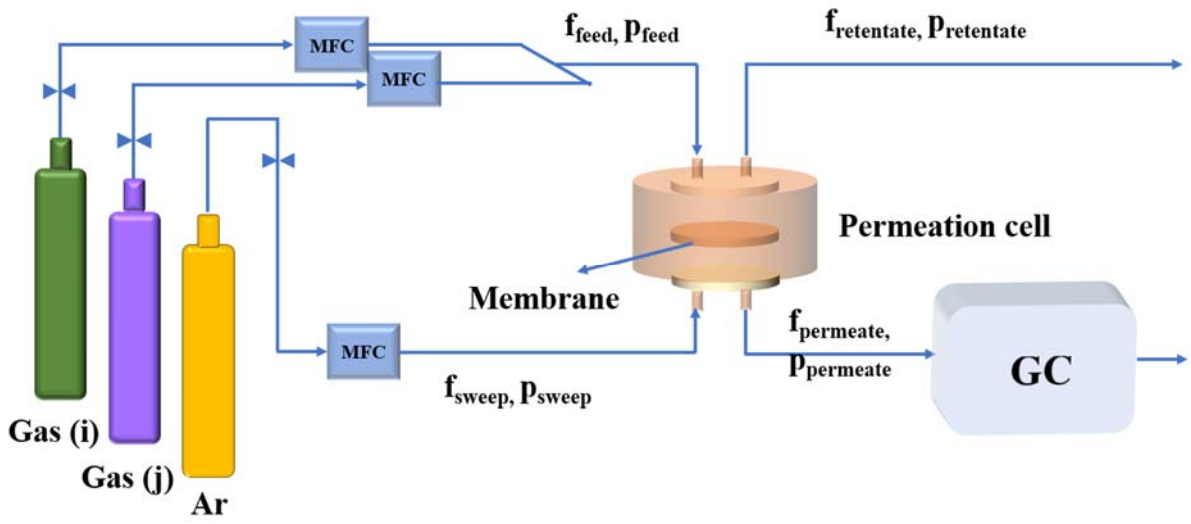

Figure S9. Measurement equipment for mixed gas permeations. MFC: mass flow controller; GC: gas chromatograph; f: volumetric flow rate; p: pressure.

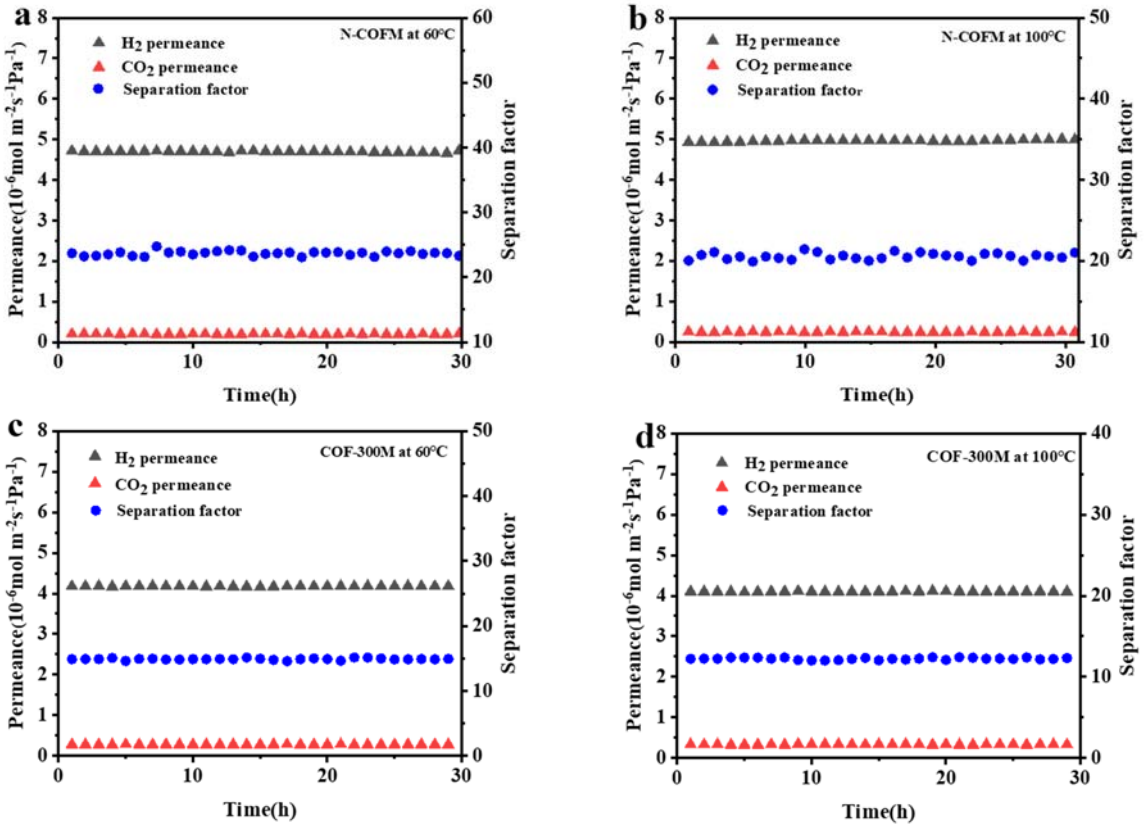

Figure S10. Long-term test of N-COF membrane (top) and COF-300 membrane (bottom) for equimolar H_2/CO_2 mixture at 60 ℃ (a and c) and 100 ℃ (b and d) and 1 bar.

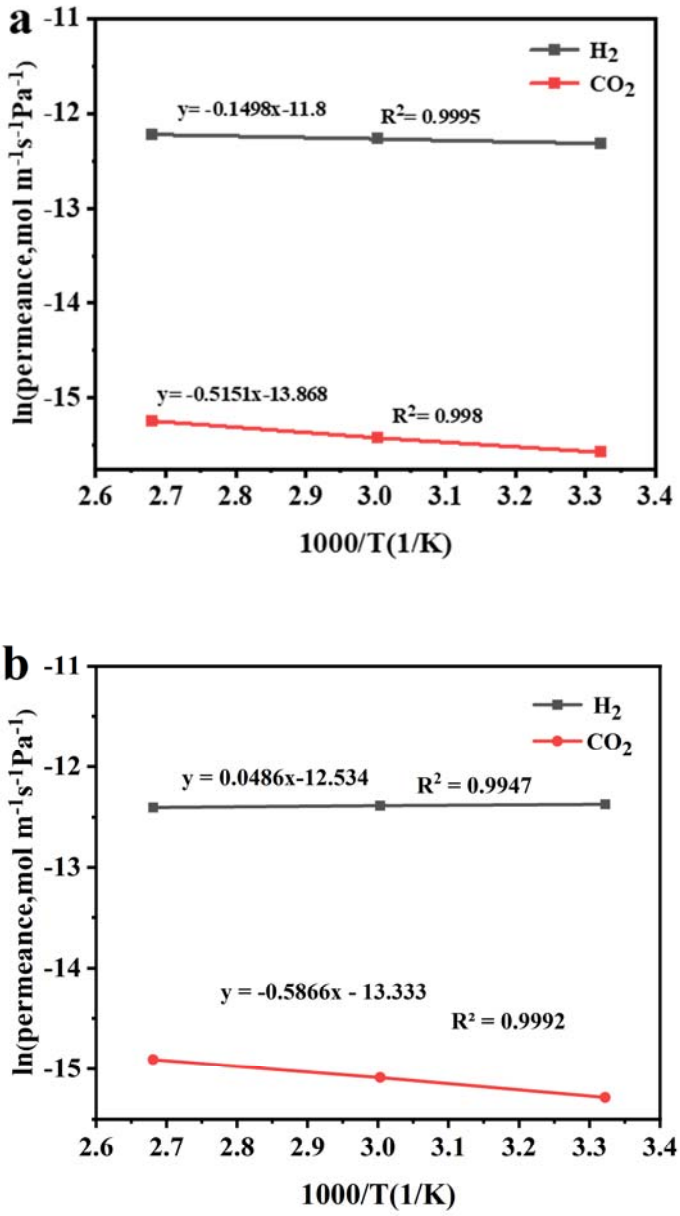

Figure S11. Arrhenius temperature dependence of H_2 and CO_2 permeance for (a) N-COF membrane and (b) COF-300 membrane.

Note: The temperature dependence of gas permeation can be described by Arrhenius equations:

$$P_i = A_i \exp(-\frac{Eact,i}{RT})$$

$$\ln(Pi) = \ln(Ai) - \frac{Eact,i}{R} \cdot \frac{1}{T}$$

where P_i is the gas permeance (mol m^{-2} s^{-1} Pa^{-1}) of component i, A_i represents the pre-exponential factor of component i, Eact,i is the apparent activation energy of component i, R is the ideal gas constant (8.314 $J \cdot mol^{-1} \cdot K^{-1}$), and T is the absolute temperature (K). The ln (P_i) versus 1/T displays a linear correlation,

of which the slope is used to calculate $E_{act,i}$. As shown in **Figure S10a**, For N-COF membrane the calculated $E_{act,CO2}$ value was 4.3 kJ/mol is higher than that of H_2 (1.2 kJ/mol). This indicates an activated diffusion process both for H_2 and CO_2 transport.

The apparent activation energy ($E_{act,i}$) is related to the diffusion activation energy (E_{diff}) and adsorption heat (Qst):

$$E_{act,i} = E_{diff} - Qst$$

where E_{diff} is the diffusion activation energy, Qst is the adsorption enthalpy. As shown in Figure S7, the higher adsorption heat of ~ 39.7 kJ/mol for CO_2 than that of ~ 7.4 kJ/mol for H_2 on N-COF membrane, the diffusion activation energy of CO_2 also higher than H_2, indicating much more activated diffusion of CO_2 through N-COF membrane.

Therefore, with the increase of temperature there is much more activated diffusion of CO_2 than H_2 in the N-COF membranes which leads to the decrease of H_2/CO_2 separation factor. Despite all of this, the overall membrane performance at 100 C° still exceeds the 2008 Robeson upper bound for H_2/CO_2.

In a similar way, as shown in **Figure S10b**, for COF-300 membrane, the calculated $E_{act, CO2}$ value was 4.9 kJ/mol, while the permeance of H_2 is basically unchanged with the change of temperature. This indicates that the activated diffusion of CO_2 is more obvious, the competitive diffusion of CO_2 at high temperature hinders the penetration of H_2. So, the selectivity of the H_2/CO_2 decreases at high temperatures. However, the overall membrane performance of the COF-300 membrane exceeds the 2008 Robeson upper bound at 100 ℃, too.

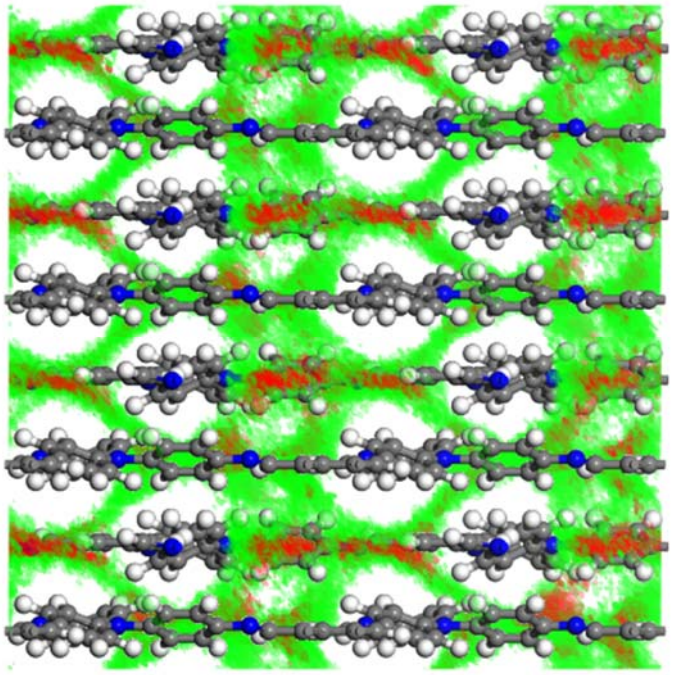

Figure S12. Density distribution contours of H_2 (red) and CO_2 (green) mixture gas in N-COF membrane (interlayer space).

Table S1. Mix gas permeances and separation factors of self-standing COFMs obtained from different synthesis batches.

Sample	Permeance (H_2) (10^{-6} mol·m^{-2}·s^{-1}·Pa^{-1})	Separation factor (H_2/CO_2)
N-COFM1	4.4669	26
N-COFM2	4.4781	22.16
N-COFM3	4.4725	24.97
COF-300M1	4.2325	18.4
COF-300M2	4.1534	20.07
COF-300M3	3.9989	17.76

Table S2. Comparison of the gas separation capabilities of reported COFMs to separate H_2/CO_2 binary mixture (1:1).

Membrane materials	$P(H_2)$	$SF(H_2/CO_2)$	Temperature (℃)	Reference
NUS-2@PBI	0.059	18.78	35	[2]
CTF-BTD/GO0.2-0.008-453	577.9	36.8	RT	[3]
COF-LZU1− ACOF-1	660.2	24.2	RT	[4]
TPPa-Me	727	12.7	RT	[5]
H2P-DHPh COF−UiO66	890.7	32.9	RT	[6]
[COF-300]-[ZIF-8]	1055.2	13.5	RT	[7]
[COF-300]-[UiO-66]	1173.1	17.2	RT	[8]
[COF-300]-[Zn2(bdc)2(dabco)]	1344	12.6	RT	[7]
DMTA-COF	1857	8.3	RT	[9]
ACOF-1	2018.9	14.1	RT	[4]
2 × (TpTGCl@TpPa-SO3H)/COF-LZU1/AAO	2163	26	150	[10]
CTF-1@GO	2534.8	22.3	RT	[11]
TpEBr@TpPa-SO3Na	2566	22.6	150	[12]
COF-300	2688	6	RT	[7]
TpPa-1-30/GO10	3144.9	25.57	RT	[13]
CTF-1@GO	3419	19.6	RT	[11]
Vertically aligned COF-LZU1	3654.8	31.6	RT	[14]
ZIF-67-in-TpPa-1	3671.1	34.9	RT	[15]
COF-LZU1	3684.2	6	RT	[4]
ZIF-67-in-TpBD	3772.7	27.9	RT	[15]
Vertically aligned TFB-BD	3802.2	25.6	RT	[14]
ZIF-8-in-TpPa-1	3920.1	23.1	RT	[15]
CTF-1@GO	5010.6	17.4	RT	[11]
Selfstanding-COF-300	**12475**	**18.4**	**RT**	**This work**
Selfsanding-N-COF	**13165**	**26**	**RT**	**This work**

[a)] $P(H_2)$ is H_2 permeance in GPU; GPU = gas permeation units; 1 GPU = 3.3928×10^{-10} mol m^{-2} s^{-1} Pa^{-1};
[b)] SF stands for separation factor.

References

[1] H. Li, J. Chang, S. Li, X. Guan, D. Li, C. Li, L. Tang, M. Xue, Y. Yan, V. Valtchev, S. Qiu, Q. Fang, *J. Am. Chem. Soc.* **2019**, *141*, 13324.

[2] Z. Kang, Y. Peng, Y. Qian, D. Yuan, M. A. Addicoat, T. Heine, Z. Hu, L. Tee, Z. Guo, D. Zhao, *Chem. Mater.* **2016**, *28*, 1277.

[3] Y. J. Zhao, P. Liu, Y. P. Ying, K. P. Wei, D. Zhao, D. H. Liu, *J. Membr. Sci.* **2021**, *632*, 119326.

[4] H. Fan, A. Mundstock, A. Feldhoff, A. Knebel, J. Gu, H. Meng, J. Caro, *J. Am. Chem. Soc.* **2018**, *140*, 10094.

[5] W. Zheng, J. Hou, C. Liu, P. Liu, L. Li, L. Chen, Z. Tang, *Chem. Asian. J.* **2021**, *16*, 3624.

[6] S. Das, T. Ben, S. Qiu, V. Valtchev, *ACS Appl. Mater. Interfaces.* **2020**, *12*, 52899.

[7] J. Fu, S. Das, G. Xing, T. Ben, V. Valtchev, S. Qiu, *J. Am. Chem. Soc.* **2016**, *138*, 7673.

[8] S. Das, T. Ben, *Dalton Trans.* **2018**, *47*, 7206.

[9] J. Fu, T. Ben, *Acta Chimica Sinica* **2020**, *78*, 805.

[10] Y. Ying, S. B. Peh, H. Yang, Z. Yang, D. Zhao, *Adv. Mater.* **2021**, 2104946.

[11] Y. Ying, D. Liu, J. Ma, M. Tong, W. Zhang, H. Huang, Q. Yang, C. Zhong, *J Mater Chem A* **2016**, *4*, 13444.

[12] Y. Ying, M. Tong, S. Ning, S. K. Ravi, S. B. Peh, S. C. Tan, S. J. Pennycook, D. Zhao, *J. Am. Chem. Soc.* **2020**, *142*, 4472.

[13] Y. Tang, S. Feng, L. Fan, J. Pang, W. Fan, G. Kong, Z. Kang, D. Sun, *Sep. Purif. Technol.* **2019**, *223*, 10.

[14] H. Fan, M. Peng, I. Strauss, A. Mundstock, H. Meng, J. Caro, *J. Am. Chem. Soc.* **2020**, *142*, 6872.

[15] H. Fan, M. Peng, I. Strauss, A. Mundstock, H. Meng, J. Caro, *Nat. Commun.* **2021**, *12*, 38.